

## Article

# A Novel Electrochemical Sensor Based on Pd Confined Mesoporous Carbon Hollow Nanospheres for the Sensitive Detection of Ascorbic Acid, Dopamine, and Uric Acid

Wanqing Zhang <sup>1,\*</sup> , Xijiao Li <sup>1</sup>, Xiaoxue Liu <sup>1</sup>, Kaixuan Song <sup>1</sup>, Haiyang Wang <sup>1</sup>, Jichao Wang <sup>1</sup> , Renlong Li <sup>1</sup>, Shanqin Liu <sup>1</sup> and Zhikun Peng <sup>2,\*</sup>

<sup>1</sup> School of Chemistry and Chemical Engineering, Henan Institute of Science and Technology, Xinxiang 453003, China; wangjichao@hist.edu.cn (J.W.)

<sup>2</sup> China Henan Institute of Advanced Technology, Zhengzhou University, Zhengzhou 450001, China

\* Correspondence: zhangwqzzu@163.com (W.Z.); zhikunpeng@zzu.edu.cn (Z.P.); Fax: +86-0373-3040933 (W.Z.)

**Abstract:** In this study, we designed a novel electrochemical sensor by modifying a glass carbon electrode (GCE) with Pd confined mesoporous carbon hollow nanospheres (Pd/MCHS) for the simultaneous detection of ascorbic acid (AA), dopamine (DA), and uric acid (UA). The structure and morphological characteristics of the Pd/MCHS nanocomposite and the Pd/MCHS/GCE sensor are comprehensively examined using SEM, TEM, XRD and EDX. The electrochemical properties of the prepared sensor are investigated through CV and DPV, which reveal three resolved oxidation peaks for AA, DA, and UA, thereby verifying the simultaneous detection of the three analytes. Benefiting from its tailorable properties, the Pd/MCHS nanocomposite provides a large surface area, rapid electron transfer ability, good catalytic activity, and high conductivity with good electrochemical behavior for the determination of AA, DA, and UA. Under optimized conditions, the Pd/MCHS/GCE sensor exhibited a linear response in the concentration ranges of 300–9000, 2–50, and 20–500  $\mu\text{M}$  for AA, DA, and UA, respectively. The corresponding limit of detection (LOD) values were determined to be 51.03, 0.14, and 4.96  $\mu\text{M}$ , respectively. Moreover, the Pd/MCHS/GCE sensor demonstrated outstanding selectivity, reproducibility, and stability. The recovery percentages of AA, DA, and UA in real samples, including a vitamin C tablet, DA injection, and human urine, range from 99.8–110.9%, 99.04–100.45%, and 98.80–100.49%, respectively. Overall, the proposed sensor can serve as a useful reference for the construction of a high-performance electrochemical sensing platform.

**Keywords:** electrochemical sensor; Pd/MCHS; ascorbic acid; dopamine; and uric acid



**Citation:** Zhang, W.; Li, X.; Liu, X.; Song, K.; Wang, H.; Wang, J.; Li, R.; Liu, S.; Peng, Z. A Novel Electrochemical Sensor Based on Pd Confined Mesoporous Carbon Hollow Nanospheres for the Sensitive Detection of Ascorbic Acid, Dopamine, and Uric Acid. *Molecules* **2024**, *29*, 2427. <https://doi.org/10.3390/molecules29112427>

Academic Editors: César Ricardo Teixeira Tarley and Roberta Antigo Medeiros

Received: 9 April 2024  
Revised: 8 May 2024  
Accepted: 17 May 2024  
Published: 21 May 2024



**Copyright:** © 2024 by the authors. Licensee MDPI, Basel, Switzerland. This article is an open access article distributed under the terms and conditions of the Creative Commons Attribution (CC BY) license (<https://creativecommons.org/licenses/by/4.0/>).

## 1. Introduction

Ascorbic acid (AA), dopamine (DA), and uric acid (UA) are small bioactive molecules that are widely distributed in human blood, urine, and the central nervous system, playing a crucial role in human metabolism and the circulatory system [1–3]. AA, as an antioxidant, participates in various biological reactions and is used as a therapeutic agent for scurvy, acquired immune deficiency syndrome (AIDS), and cancers [4–6]. DA is an excitatory neurotransmitter, regulating endocrine as well as mental and physical activities. A lack of DA can cause heart disease, Parkinson’s disease, and other neurological diseases in humans [7,8]. UA is the primary end product of the metabolic breakdown of purine nucleotides, and it is one of the most important antioxidants in human fluids, such as urine and serum. Excessive UA in the human body can cause several diseases, such as gout, hypertension, arthritis, and hyperuricemia [9–11]. Therefore, there is an urgent need to develop a rapid, sensitive, and reliable method for the simultaneous detection of AA, DA and UA, considering their concurrent presence in physiological processes [12–15].

Until now, numerous analytical techniques have been applied for the detection of AA, DA, and UA, such as fluorescence spectroscopy [16,17], colorimetry [18,19], capillary

electrophoresis [20,21], and high-performance liquid chromatography [22]. Despite achieving excellent reproducibility, wide detection range, and high accuracy, these conventional methods require complex separation processes, a high level of professionalism, and time-consuming procedures, limiting their broader application. By contrast, the electrochemical methods offer numerous advantages, including simple operation, rapid response, high sensitivity, low cost, and high feasibility, demonstrating their potential in the rapid detection of trace target molecules [23–25]. However, when AA, DA, and UA coexist in a sample, their oxidation peak potentials usually overlap when using bare glassy carbon electrode (GCE), so it is difficult to detect them simultaneously. To address this issue, novel electrode materials have been developed by modifying GCE for the distinguishing of these three analytes, such as metal oxide/carbon composite material [26], nitrogen–carbon material [27], and carbon matrix composite material [28].

A mesoporous carbon hollow sphere (MCHS) is a three-dimensional carbon material with large cavities and porous carbon shells, exhibiting uniform geometry, tunable porosity, a large surface area, and small particle size [29,30]. Consequently, it has been widely applied in catalysis [31], supercapacitors [32], drug release [33], batteries [34], and energy storage [35]. Palladium (Pd) nanoparticles, as noble metal nanomaterials, have garnered considerable research interest owing to their excellent catalytic activity, cost-effectiveness, and abundant availability. Nonetheless, the small size of Pd nanoparticles increases their surface free energy, causing their aggregation into larger nanoparticles. This leads to a significant decline in both the catalytic activity and stability of the resultant nanocomposite [36,37]. In the structure, metallic Pd nanoparticles are dispersed in the network of an MCHS, which not only affords a boost to conductivity but also greatly alleviates the aggregation of active sites. Simultaneously, the unique hollow structure facilitates the efficient mass transport and shortens the transmission path of electrons in the nanocomposite. Notably, nitrogen atoms within the MCHSs expose additional active sites that coordinate with Pd nanoparticles, forming robust Pd–N bonds [38]. This ensures the tight anchoring of Pd nanoparticles, endowing the nanocomposite with exceptional stability and electrochemical performance [39,40]. This feature can be helpful in the detection of AA, DA, and UA. However, to the best of our knowledge, the modification of GCE with a Pd-doped MCHS (Pd/MCHS) to realize the simultaneous determination of the three analytes has not yet been reported.

In this study, we applied a GCE modified with a Pd/MCHS nanocomposite for the concurrent detection of AA, DA, and UA. The distinctive hollow cavity structure of an MCHS not only facilitated the uniform dispersion of Pd nanoparticles but also prevented their aggregation during the fabrication process. The prepared Pd/MCHS/GCE sensor exhibited excellent sensitivity and selectivity in the individual detection of each analyte as well as in the simultaneous detection of the triad. According to the above considerations, the electrochemical sensor based on the Pd/MCHS nanocomposite proposed in this paper provides an efficient and sensitive method for the detection of biological small molecules, broadens the application range of the Pd/MCHS nanocomposite, and enriches the sensing mechanism in the field of biological sensors.

## 2. Results and Discussion

### 2.1. Characterization of Pd/MCHS

SEM and TEM were used to reveal the microscopic morphologies of the Pd/MCHS/GCE and Pd/MCHS nanocomposites. The SEM image in Figure 1a shows that the Pd/MCHS/GCE has regular spherical morphology with a rough surface. The electrode surface appears as a broken ball, indicating that the nanocomposite has a hollow mesoporous structure with a size of approximately 345 nm, which contains uniformly dispersed Pd nanoparticles [41]. This arrangement significantly enhances the surface area of the Pd/MCHS material. According to the TEM image in Figure 1b, the Pd/MCHS nanocomposite exhibits a uniform spherical structure, where the diameter of spheres is approximately 362 nm, the diameter of the hollow structure is approximately 220 nm, and the thickness of the porous

carbon shell is approximately 71 nm. Moreover, the Pd nanoparticles are evenly distributed within the MCHS material, avoiding particle aggregation, which highlights the outstanding anchoring capability of an MCHS. Notably, the hollow carbon nanosphere structure of the Pd/MCHS nanocomposite provides additional active sites through radical channels, facilitating electrode/electrolyte contact and enhancing the electrochemical performance of the prepared sensor [35].

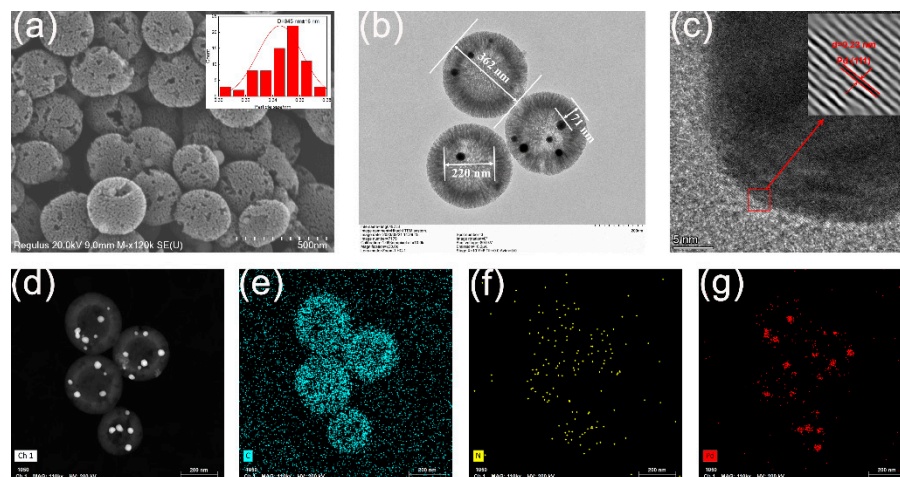


**Figure 1.** (a) SEM (inset: size distribution), (b) TEM, (c) HRTEM, and (d–g) elemental mapping images of Pd/MCHS nanocomposite.

In the high-resolution TEM (HRTEM) image of the Pd/MCHS nanocomposite (Figure 1c), an obvious interplanar spacing of 0.23 nm, corresponding to Pd (111), is observed for the ultrafine Pd nanoparticles. This indicates a face-centered cubic (fcc) structure of the Pd crystal lattice [29,42]. The elemental distribution of the Pd/MCHS nanocomposite was examined through EDS. The element mapping images in Figure 1d–g verify the homogeneous distribution of C, O, N, and Pd across the Pd/MCHS framework. Remarkably, the Pd nanoparticles are uniformly dispersed in the Pd/MCHS nanocomposite without any aggregation. These findings validate the successful synthesis of finely dispersed Pd nanoparticles firmly anchored onto the electrocatalytic substrate.

The crystal structure of the Pd/MCHS nanocomposite was examined by XRD, and the results are shown in Figure 2. The sample exhibits a distinct diffraction peak at  $24.6^\circ$ , which is attributed to the (002) facet of graphitic carbon, confirming the presence of an amorphous structure. Furthermore, the fcc structure of the Pd crystal is confirmed by the diffraction peaks at  $40.0^\circ$ ,  $46.0^\circ$ , and  $68.0^\circ$ , corresponding to the (111), (200), and (220) facets, respectively [43].

XPS was employed to further verify the successful fabrication of the Pd/MCHS nanocomposite. The peaks corresponding to C, N, and Pd are evident in the XPS spectrum of nanocomposite (Figure 3a). The results were consistent with the EDS elemental mapping. The high-resolution C 1s spectrum shows distinct peaks corresponding to different carbon bonds:  $sp^2$  C=C at 284.6 eV, C-N at 285.4 eV, C=O at 286.9 eV, and COOH at 289.5 eV (Figure 3b). Furthermore, the N 1s spectra exhibits discernible peaks representing pyridinic N (397.58 eV), Pd–N (399.5 eV), pyrrolic N (400.54 eV), and oxidized nitrogen species (405.3 eV) (Figure 3c). Notably, the interaction between pyridine N and Pd nanoparticles (Pd–N) is strong, which is ascribed to the more negative charges and diffuse orbitals associated with pyridine N. This interaction can effectively prevent the agglomeration of Pd nanoparticles, thereby enhancing the electrocatalytic activity and stability of the Pd/MCHS nanocomposite. The Pd 2p spectrum reveals a pair of peaks at 335.6 and 341.0 eV, which correspond to the metallic Pd (PdO) in the Pd/MCHS nanocomposite. Additionally, the peaks at 338.0 and 343.3 eV are attributed to the Pd–N interaction or PdO species (Figure 3d) [39].

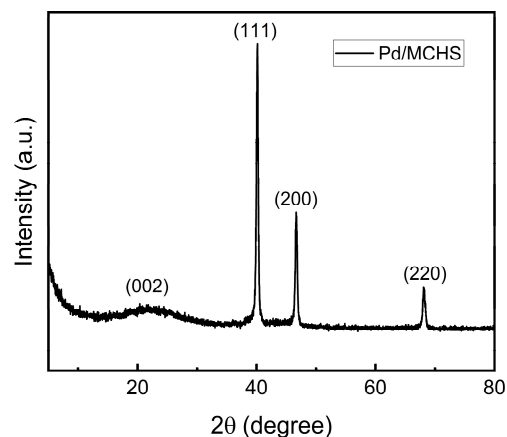


**Figure 2.** XRD pattern of Pd/MCHS nanocomposite.

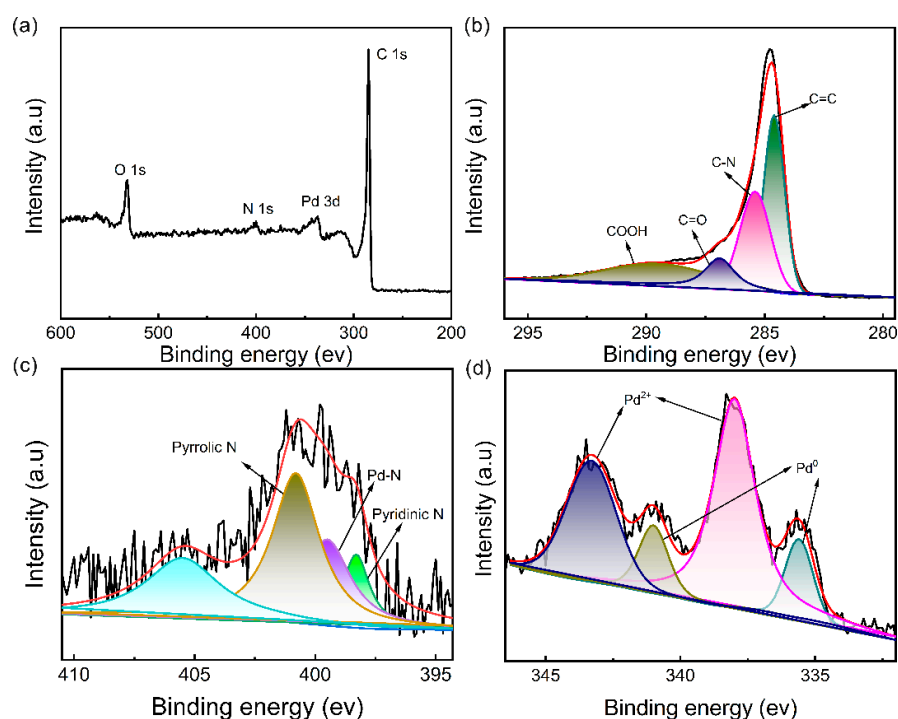


**Figure 3.** (a) XPS survey spectra of Pd/MCHS nanocomposite and high-resolution spectra of (b) C 1s, (c) N 1s, and (d) Pd 2p.

## 2.2. Electrochemical Behavior of the Pd/MCHS/GCE Sensor

CV was employed to assess the interfacial charge transfer properties of GCE and the Pd/MCHS/GCE sensor. As illustrated in Figure 4a, distinct redox peaks are evident in the CV curve of unmodified GCE, which indicates the quasi-reversible electrochemical response of  $\text{Fe}(\text{CN})_6^{3-/4-}$ . The modification of the GCE surface with Pd/MCHS results in a significant increase in the redox peak current. This suggested that the Pd/MCHS/GCE sensor had a large electrochemical active area, which can be ascribed to the synergistic effect of MCHS and Pd nanoparticles in promoting the electron transfer ability.

EIS is an effective method for evaluating the electrochemical features of a sensor by monitoring the changes in the charge transfer resistance ( $R_{ct}$ ) on the electrode surface. As shown in Figure 4b, an obvious semicircle is observed in the high frequency region of GCE. After the modification with the Pd/MCHS material, the semicircle diameter notably decreases. This reduction can be attributed to the enhanced electrical conductivity of the Pd/MCHS nanocomposite, facilitating the transfer of electrons in the redox reaction. The



to be 0.0206 and 0.115 cm<sup>2</sup>. The effective surface area of the proposed sensor was obviously increased, which is conducive to the enrichment of target molecules on the sensor, the occurrence of electrochemical reactions, and the sensitive detection of small biological molecules [46–48].

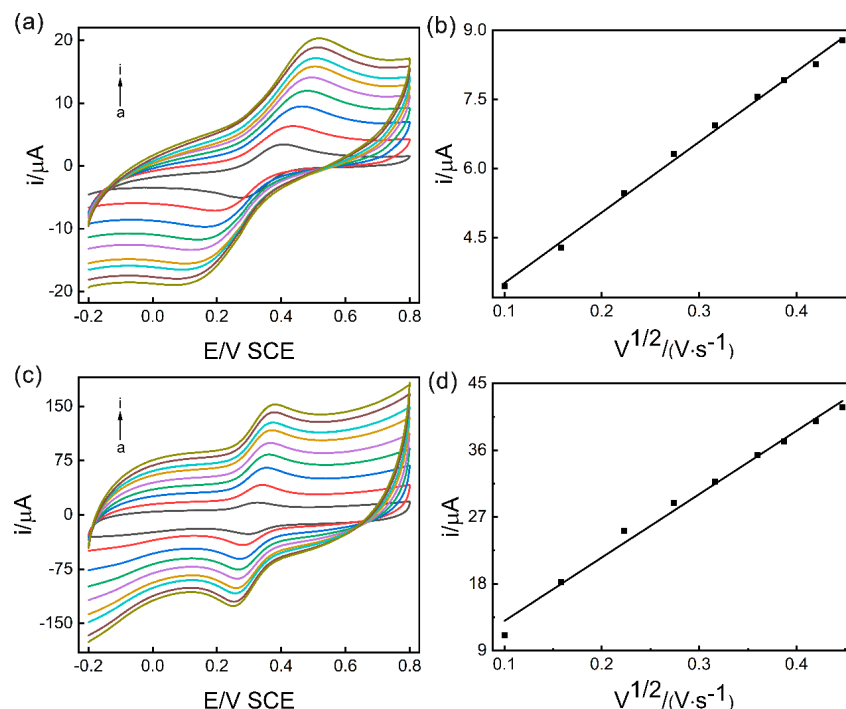


**Figure 6.** CV curves of GCE (a) and Pd/MCHS/GCE sensor (c) in 0.1 M of KCl solution containing 1 mM  $[\text{Fe}(\text{CN})_6]^{3-/4-}$ . Linear relationship between the peak current ( $I_p$ ) and the square root of the scan rate of GCE (b) and Pd/MCHS/GCE sensor (d).

The recognition mechanism of the Pd/MCHS/GCE sensor for the three target molecules is described as follows. The Pd/MCHS nanocomposite can provide abundant surface active sites, increase the collision probability between materials and target molecules, and finally enhance the detection signal of target molecules. Furthermore, the N doping in the Pd/MCHS nanocomposite improves the catalytic activity and biocompatibility of the materials, so that the electrons can be efficiently transferred between the Pd/MCHS/GCE sensor and the target molecules, which is conducive to the sensitive detection of AA, DA, and UA. The Pd/MCHS nanocomposite provides a favorable microenvironment to the target analyte. A small amount of AA, DA, and UA can trigger the composite to release a large number of signal molecules, resulting in a strong response signal, thereby achieving the rapid detection of AA, DA, and UA.

### 2.3. Optimization of Experimental Conditions

#### 2.3.1. Effect of Different Buffer Solutions

The electrochemical behavior of AA, DA and UA on the Pd/MCHS/GCE sensor depends on various factors, such as the type of supporting buffer solution, pH value, the amount of Pd/MCHS nanocomposite, and scan rate. To obtain the optimal supporting buffer solution, the CV method was utilized to examine the oxidation behavior of AA, DA, and UA in PBS (i), citric acid-sodium citrate buffer solution (ii), Britton–Robinson (B–R) solution (iii), acetic acid sodium acetate buffer solution (ABS) (iv), and glycine-hydrochloric acid buffer solution (v), and the results are shown in Figure 7. Compared with the other four buffer solutions, PBS exhibited the highest electrochemical response in the detection of AA, DA and UA, and the corresponding peak currents are 36.24, 44.08, and 48.43  $\mu\text{A}$ , respectively. Therefore, PBS was chosen as the buffer solution in the subsequent measurements.

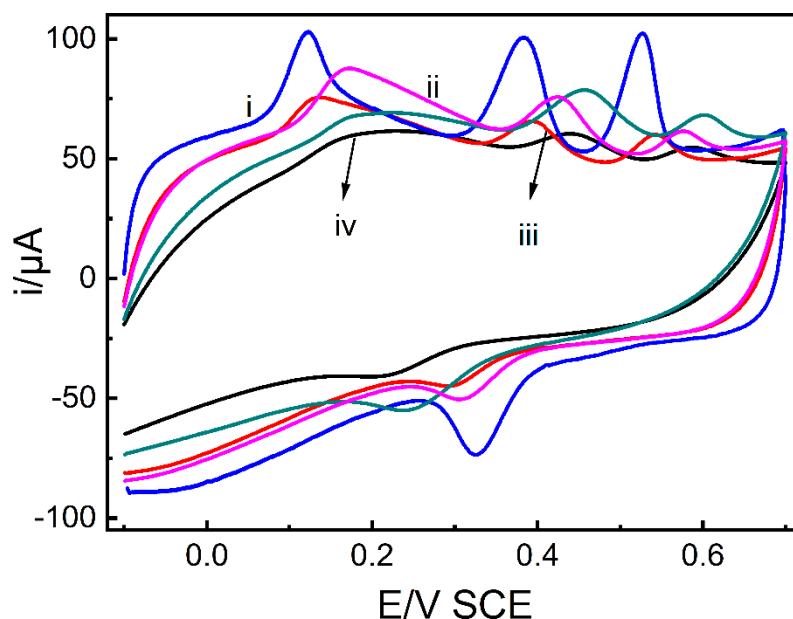


**Figure 7.** Effect of supporting electrolyte type on the sensor response: (i) PBS, (ii) citric acid-sodium citrate buffer solution, (iii) Britton–Robinson (B–R) solution, (iv) ABS, and (v) glycine-hydrochloric acid buffer solution.

### 2.3.2. Effect of pH

The impact of buffer pH on the current response of the Pd/MCHS/GCE sensor for the determination of 1000  $\mu\text{M}$  AA, 40  $\mu\text{M}$  DA, and 80  $\mu\text{M}$  UA, was systematically investigated over a range of pH values from 2.5 to 5, and the results are shown in Figure 8a. It can be seen in Figure 8b that the peak potential ( $E_p$ ) exhibited a discernible negative shift as the pH of the electrolyte increases. This indicated a concurrent electron and proton transfer during the electrochemical oxidation reaction [49,50]. The relationship between  $E_p$  and pH can be expressed as follows:  $E_p$  (V) = 0.0503 pH + 0.294 ( $R^2 = 0.995$ ) for AA,  $E_p$  (V) = 0.0347 pH + 0.513 ( $R^2 = 0.995$ ) for DA, and  $E_p$  (V) = 0.0383 pH + 0.668 ( $R^2 = 0.993$ ) for UA. Figure 8c further illustrates that the peak currents of these analytes depend on the pH value of the buffer solution. Consequently, 0.1 M PBS at pH 3.0 was selected as the supporting electrolyte solution for this experiment.

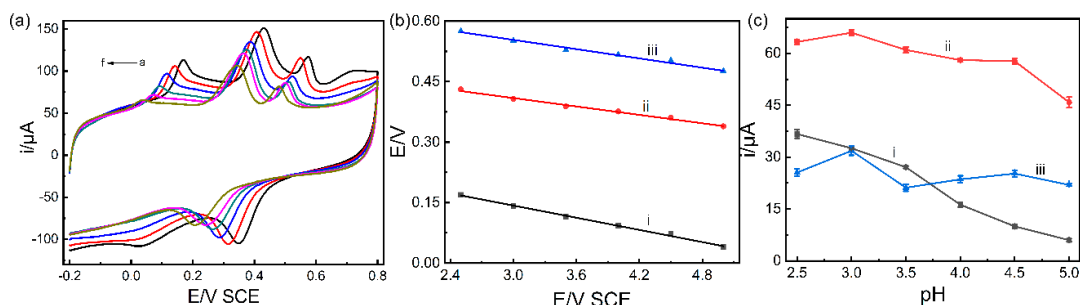


**Figure 8.** (a) CV curves for the oxidation of AA (1000  $\mu\text{M}$ ), DA (40  $\mu\text{M}$ ), and UA (80  $\mu\text{M}$ ) on the Pd/MCHS/GCE sensor under various pH values ranging from 2.5 to 5 (a–f); (b) influence of pH on the oxidation peak potentials; (c) influence of pH on the oxidation peak current: (i) AA; (ii) DA, and (iii) UA.

### 2.3.3. Effect of the Amount of Pd/MCHS

The optimal loading amount of Pd/MCHS material on the GCE electrode was investigated through seven control experiments using different amounts of Pd/MCHS (2, 4, 6, 8, 10, 12, and 14  $\mu\text{L}$ ). It can be seen in Figure 9 that, as the amount of Pd/MCHS increases, the

peak current of AA, DA, and UA grows dramatically and reaches its maximum value at 6  $\mu\text{L}$ . Then, the current response rapidly decreases with a further increase in the amount of Pd/MCHS. This may be because the elevated amount of Pd/MCHS leads to its aggregation, which hinders the interfacial transport of electrons. These results suggested that 6  $\mu\text{L}$  was the optimal amount of Pd/MCHS for the oxidation of AA, DA, and UA on the Pd/MCHS/GCE sensor.

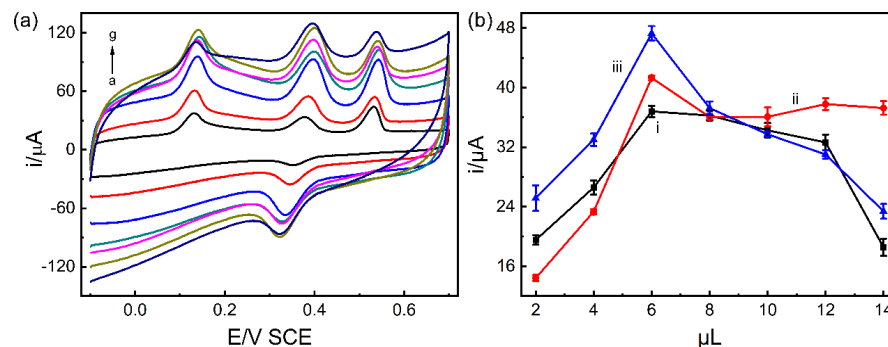


**Figure 9.** (a) CV curves for the oxidation of AA (1000  $\mu\text{M}$ ), DA (40  $\mu\text{M}$ ), and UA (80  $\mu\text{M}$ ) on the Pd/MCHS/GCE sensor under different amounts of modifier ranging from 2  $\mu\text{L}$  to 14  $\mu\text{L}$  (a–g). (b) Effect of the amount of Pd/MCHS dispersion on the oxidation peak current: (i) AA, (ii) DA, and (iii) UA.

#### 2.3.4. Effect of Scan Rate

Figure 10a shows the electrochemical response of the Pd/MCHS/GCE sensor in 0.1 M PBS (pH 3.0) solution containing 1000  $\mu\text{M}$  AA, 40  $\mu\text{M}$  DA, and 80  $\mu\text{M}$  UA at different scan rates. As the scan rate increases from 10 to 250  $\text{mV}\cdot\text{s}^{-1}$ , both oxidation and reduction peak currents increase linearly. Figure 10b–d displays the linear relationship between the peak current ( $I$ ) and scan rate ( $v$ ), which can be described using the following regression equations:  $I_{\text{AA}} = 0.283 C_{\text{AA}} + 15.923$  ( $R^2 = 0.999$ ),  $I_{\text{DA}} = 0.612 C_{\text{DA}} + 0.011$  ( $R^2 = 0.999$ ), and  $I_{\text{UA}} = 0.506 C_{\text{UA}} + 3.541$  ( $R^2 = 0.999$ ). These findings indicated that the electrochemical oxidation process of the Pd/MCHS/GCE sensor toward AA, DA, and UA follows a surface-controlled mechanism [51].

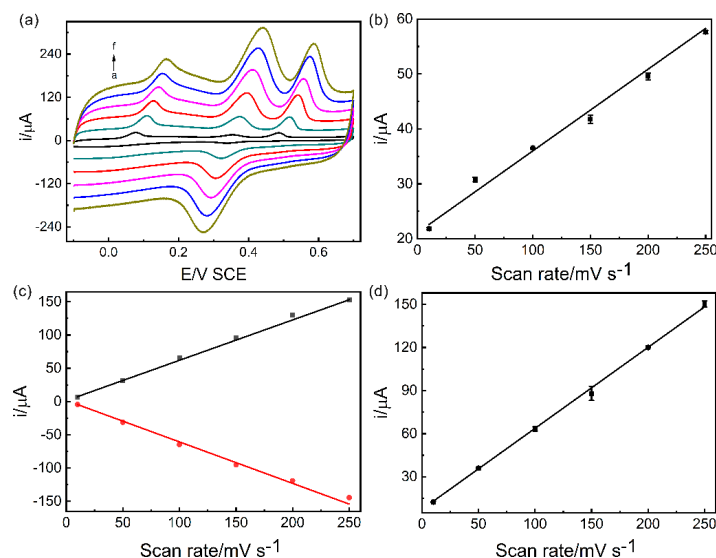


**Figure 10.** (a) CV curves of Pd/MCHS/GCE sensor in PBS (pH = 3.0, 0.1 M) containing 1000  $\mu\text{M}$  AA, 40  $\mu\text{M}$  DA, and 80  $\mu\text{M}$  UA under scan rates from 10 to 250  $\text{mV}\cdot\text{s}^{-1}$  (a–f). A linear relationship is observed between the oxidation peak current and scan rates: (b) AA, (c) DA, and (d) UA.

The above experiments were used to determine the optimal conditions for the application of the Pd/MCHS/GCE sensor in the electrochemical detection of AA, DA, and UA.

### 2.3.5. Selection of Analytical Method

In order to select the best technique method, square wave voltammetry (SWV) and differential pulse voltammetry (DPV) were used to investigate the effects of the Pd/MCHS/GCE sensor with an AA, DA and UA mixed solution, and the obtained signals are shown in Figure 11. The working parameters of SWV were as follows: the amplitude was 25 mV, the frequency was 15 Hz; the DPV had an amplitude of 50 mV and a pulse width of 200 mV. Because the three compounds exhibited higher peak currents and better peak shape in when separated further and further, DPV was used to analyze AA, DA, and UA in the following experiments.

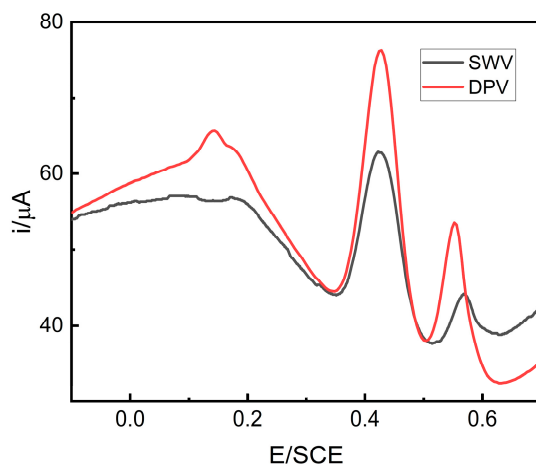


**Figure 11.** Selection of an analytical method for the detection of AA, DA, and UA.

### 2.4. Individual and Simultaneous Determination of AA, DA, and UA

DPV with high sensitivity and resolution was employed for the determination of AA, DA, and UA under optimal conditions. As depicted in Figure 12a,c,e, when keeping the concentrations of the two analytes constant while increasing the concentration of the third analyte, a consistent variation in the peak current value of the third analyte was observed. As seen in Figure 12b,d,f, the linear relationship between the peak current value ( $I_p$ ) and concentration ( $C$ ) can be described by the following equations:  $I_p$  ( $\mu\text{A}$ ) = 0.00269  $C_{AA}$  ( $\mu\text{M}$ ) + 15.940,  $I_p$  ( $\mu\text{A}$ ) = 2.644  $C_{DA}$  ( $\mu\text{M}$ ) - 1.757,  $I_p$  ( $\mu\text{A}$ ) = 1.145  $C_{DA}$  ( $\mu\text{M}$ ) + 14.436, and  $I_p$  ( $\mu\text{A}$ ) = -0.198  $C_{UA}$  ( $\mu\text{M}$ ) + 0.039. The limit of detection (LOD) values were calculated to be 31.10, 0.036, and 5.00  $\mu\text{M}$ , respectively.

When varying the AA concentration and keeping the DA and UA concentrations constant, AA is more likely to form a stable adsorption layer in the Pd/MCHS/GCE sensor. DA and UA will compete with AA for the adsorption site on the sensor, and continue to be crowded out, affecting their mass transmission and diffusion behavior, which resulted in its peak current increasing with the change of concentration. The same current changes occurred when DA and UA concentrations change.

Furthermore, the concurrent detection of AA, DA and UA with different concentrations was thoroughly examined under the optimal experimental conditions. Figure 13 shows the variation in the current response as a function of the concentrations of AA, DA, and UA. The linear concentration ranges for AA, DA, and UA were determined to be 300–9000  $\mu\text{M}$ , 2–50  $\mu\text{M}$ , and 20–500  $\mu\text{M}$ , with LOD values of 51.00, 0.14, and 4.96  $\mu\text{M}$ , respectively. These findings demonstrated that the Pd/MCHS/GCE sensor can accurately determine AA, DA, and UA.

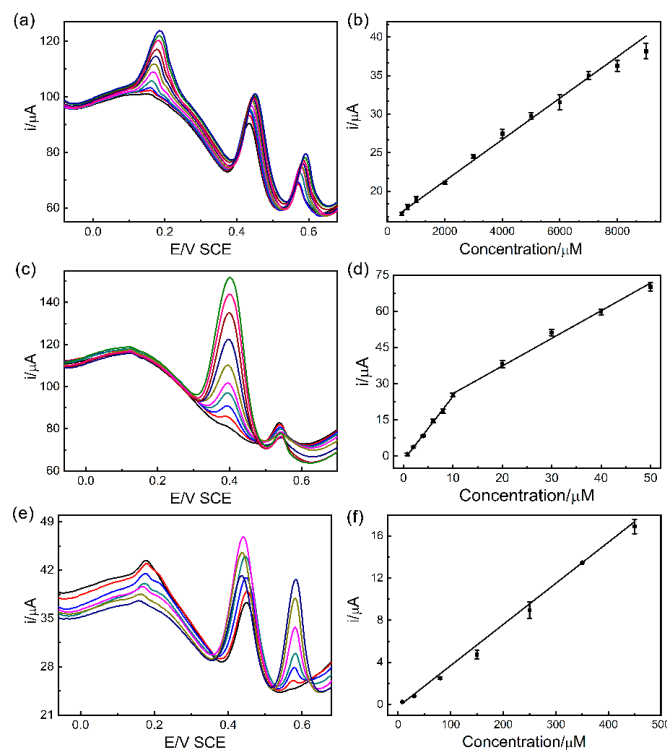


**Figure 12.** DPV curves of Pd/MCHS/GCE sensor in PBS (pH = 3.0, 0.1 M) solution containing (a) 10  $\mu\text{M}$  DA, 200  $\mu\text{M}$  UA, and different concentrations of AA from 500 to 9000  $\mu\text{M}$ ; (c) 1000  $\mu\text{M}$  AA, 200  $\mu\text{M}$  UA, and different concentrations of DA from 0.5–10  $\mu\text{M}$  to 10–50  $\mu\text{M}$ ; (e) 1000  $\mu\text{M}$  AA, 10  $\mu\text{M}$  DA, and different concentrations of UA from 8 to 450  $\mu\text{M}$ . A linear relationship is observed between  $I_p$  and the corresponding concentration (C) of (b) AA, (d) DA, and (f) UA.

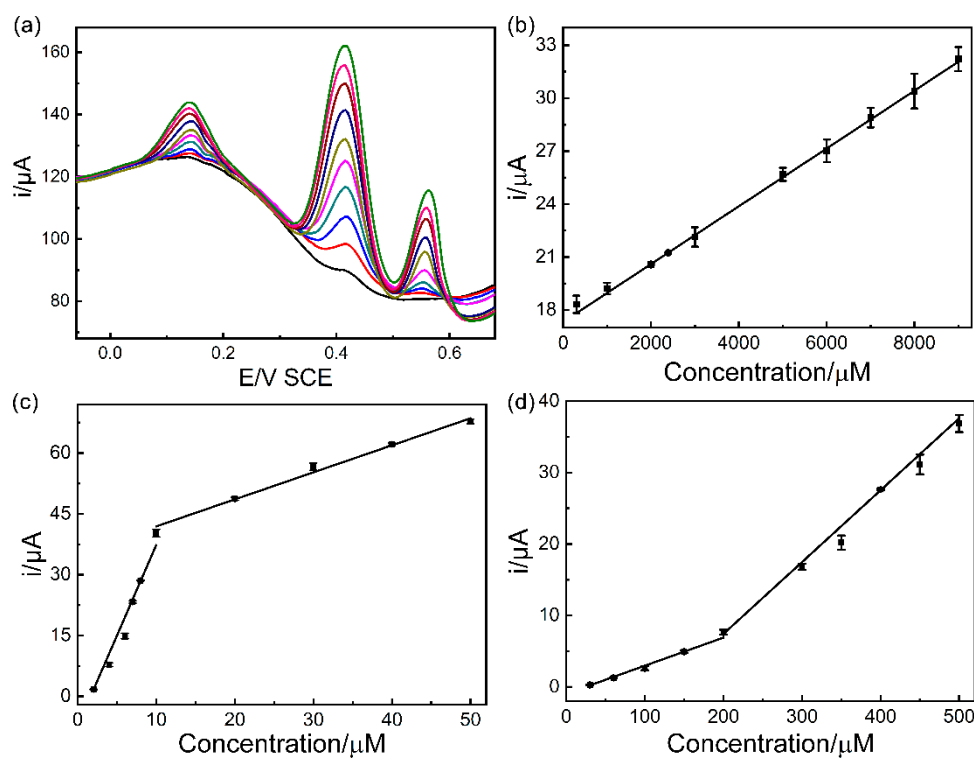


**Figure 13.** (a) DPV curves of Pd/MCHS/GCE sensor in PBS (pH = 3.0, 0.1 M) solution containing 300–9000  $\mu\text{M}$  AA, 2–50  $\mu\text{M}$  DA, and 20–500  $\mu\text{M}$  UA. A linear relationship is observed between the peak current ( $I_p$ ) and concentration (C) of (b) AA, (c) DA, and (d) UA.

A comparative analysis with other sensors revealed that the Pd/MCHS/GCE sensor exhibited a desirable linear range for the measurement of AA, DA, and UA (Table 1). Notably, the proposed sensor demonstrated a relatively lower LOD, which is attributed to the abundant surface active sites, excellent electrical conductivity, and suitable N doping in the Pd/MCHS nanocomposite. Overall, with a straightforward electrochemical assembly strategy, a novel sensing platform with a Pd/MCHS modified electrode can be constructed, which displayed remarkable performance for the detection of AA, DA, and UA.

**Table 1.** Comparison between the electrochemical performance of the proposed and other reported electrode sensors for the detection of AA, DA, and UA.

Electrode	Linear Range ( $\mu\text{M}$ )			Limit of Detection ( $\mu\text{M}$ )			Refs.
	AA	DA	UA	AA	DA	UA	
MWCNT-PEDOT/GCE	100–2000	10–330	10–250	100	10	10	[28]
ERGO/GCE	500–2000	0.5–60	0.5–60	250	0.5	0.5	[52]
Bare GCE	0–190	0–160	0–100	7.66	11.34	5.63	[53]
SDS/CPE	-	10–196	60–654	-	7.71	35.88	[54]
GEF/CFE	73.52–2305.53	1.36–125.69	3.98–371.49	73.52	1.36	3.98	[55]
Au-RGO/GCE	240–1500	6.8–41	8.7–53	51	1.4	1.8	[56]
Pd/MCHS/GCE <sup>a</sup>	500–9000	0.8–50	8–450	31.10	0.036	5.00	This work
Pd/MCHS/GCE <sup>b</sup>	300–9000	2–50	20–50	51.00	0.14	4.96	This work

<sup>a</sup> Individual analysis; <sup>b</sup> Simultaneous analysis.

### 2.5. Reproducibility, Stability, and Anti-Interference Performance of Pd/MCHS/GCE Sensor

The reproducibility and stability of the Pd/MCHS/GCE sensor were investigated in a 0.1 M PBS solution with a pH of 3.0, containing 1000  $\mu\text{M}$  AA, 40  $\mu\text{M}$  DA, and 80  $\mu\text{M}$  UA using DPV technology under the optimal conditions. The reproducibility of the sensor was evaluated by fabricating six identical modified electrodes for the mixed solution, ensuring consistency in the manufacturing process. As shown in Table 2, the average relative standard deviation (RSD) for AA, DA, and UA are 4.60%, 1.96%, and 2.82%, respectively, signifying the excellent reproducibility of the Pd/MCHS/GCE sensor. Furthermore, the fabricated sensor was maintained at 4 °C for 10 days to evaluate its stability, and the current response of the electrode was randomly monitored at 1, 3, 5, 7, and 10 days. As shown in Figure 14, after storage for 10 days, the peak current density of AA, DA, and UA decreased by only 12.64%, 12.40%, and 10.83%, respectively, verifying the excellent stability of the Pd/MCHS/GCE sensor.

**Table 2.** Oxidation currents of 1000  $\mu\text{M}$  AA, 40  $\mu\text{M}$  DA, and 80  $\mu\text{M}$  UA with six independent sensors.

	$i_1$ ( $\mu\text{A}$ )	$i_2$ ( $\mu\text{A}$ )	$i_3$ ( $\mu\text{A}$ )	$i_4$ ( $\mu\text{A}$ )	$i_5$ ( $\mu\text{A}$ )	$i_6$ ( $\mu\text{A}$ )	RSD (%)
AA	30.84	32.73	33.00	34.72	34.54	34.67	4.60
DA	50.90	49.96	50.25	48.46	48.75	48.92	1.96
UA	52.14	51.89	51.23	49.95	49.58	48.53	2.82

To confirm the high selectivity of the Pd/MCHS/GCE sensor for the determination of AA, DA, and UA, the recognition performance of the sensor for different substances ( $\text{KNO}_3$ ,  $\text{Na}_2\text{SO}_4$ ,  $\text{Ca}(\text{NO}_3)_2$ , sucrose, citric acid, and glucose) was investigated under a voltage of 0.1 V (AA), 0.4 V (DA), and 0.55 V (UA), and the results were shown in Figure 15. Compared to the current signal obtained from AA (1000  $\mu\text{M}$ ), DA (30  $\mu\text{M}$ ), and UA (30  $\mu\text{M}$ ), the interfering species (2000  $\mu\text{M}$ ) do not induce an obvious current response. Due to the attractive electronic properties and high catalytic activity of the Pd/MCHS nanocomposite, it can provide electron tunneling, enabling electrons to transfer between the active site of the nanocomposite and the Pd/MCHS/GCE sensor, and can selectively improve the mass diffusion of the target molecule, so that the constructed electrochemical sensor shows a

highly sensitive and selective electrochemical sensing performance in the detection of AA, DA and UA.

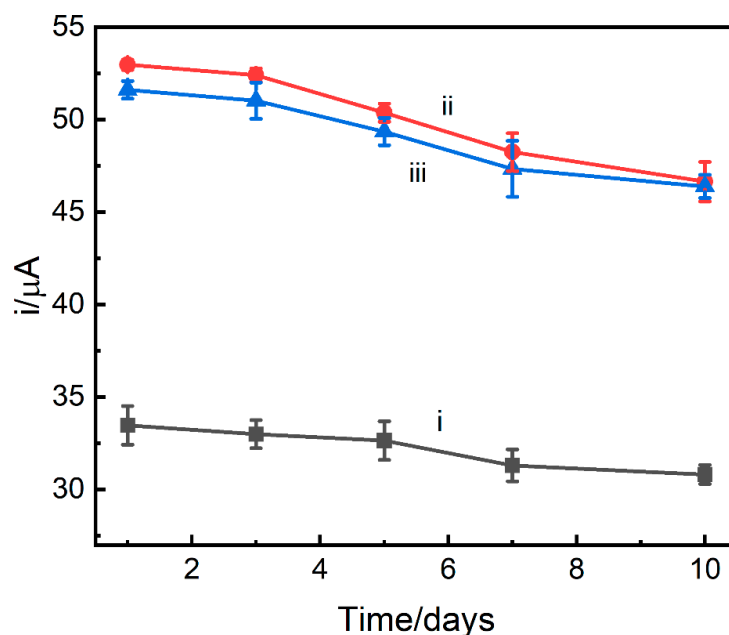


**Figure 14.** Stability of Pd/MCHS/GCE sensor toward 1000  $\mu\text{M}$  AA (i), 40  $\mu\text{M}$  DA (ii), and 80  $\mu\text{M}$  UA (iii) for 10 days.

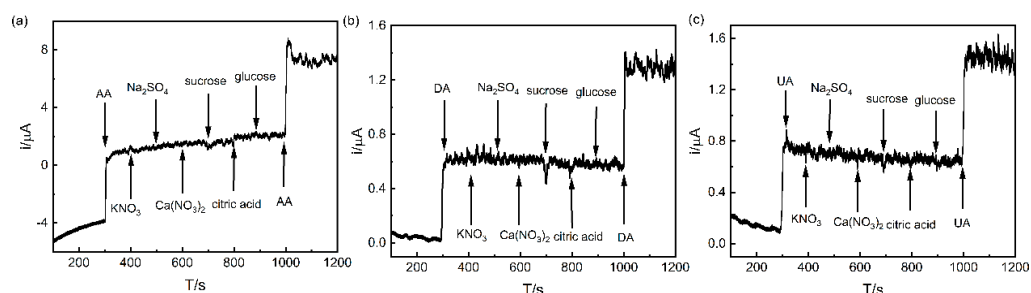


**Figure 15.** Selectivity of the Pd/MCHS/GCE sensor toward AA (a), DA (b), and UA (c) in the presence of different interfering species including  $\text{KNO}_3$ ,  $\text{Na}_2\text{SO}_4$ ,  $\text{Ca}(\text{NO}_3)_2$ , sucrose, citric acid, and glucose.

The amperometry method is an electrochemical method for the quantitative analysis of electrochemically active substances by applying a constant potential to the study electrode. Because this method can maintain constant potential and reduce the influence of the double layer charging current, it is often used to detect real samples. Therefore, it was used to detect AA, DA, and UA in a vitamin C tablet, DA injection, and human urine to assess the practical feasibility of the Pd/MCHS/GCE sensor. The specific parameters were set as follows: the initial potential was 0.55 V, the sampling interval was 0.1 s, and the sampling time was 1600 s. As shown in Figure 16, the recoveries were calculated based on the relationship between  $\Delta C$  and  $\Delta I$ . The average recoveries of AA, DA, and UA in the Pd/MCHS/GCE sensor were 99.8–110.9%, 99.04–100.45%, and 98.80–100.49%, respectively.

In order to verify the reliability of the electrochemical sensor method, the data of real samples detected using a UV–Vis spectrophotometer were used for comparison. The maximum absorption wavelengths of ascorbic acid and uric acid were 280 nm and 400 nm, respectively. By drawing standard curves and adopting a standard addition method, the recoveries of ascorbic acid and uric acid were in the range of 98.10–100.25% and 100.36–101.82% (Table 3), respectively, which was consistent with the data of real samples

detected using the electrochemical sensor method, indicating that the electrochemical detection of AA, DA and UA contents in real samples had strong feasibility.

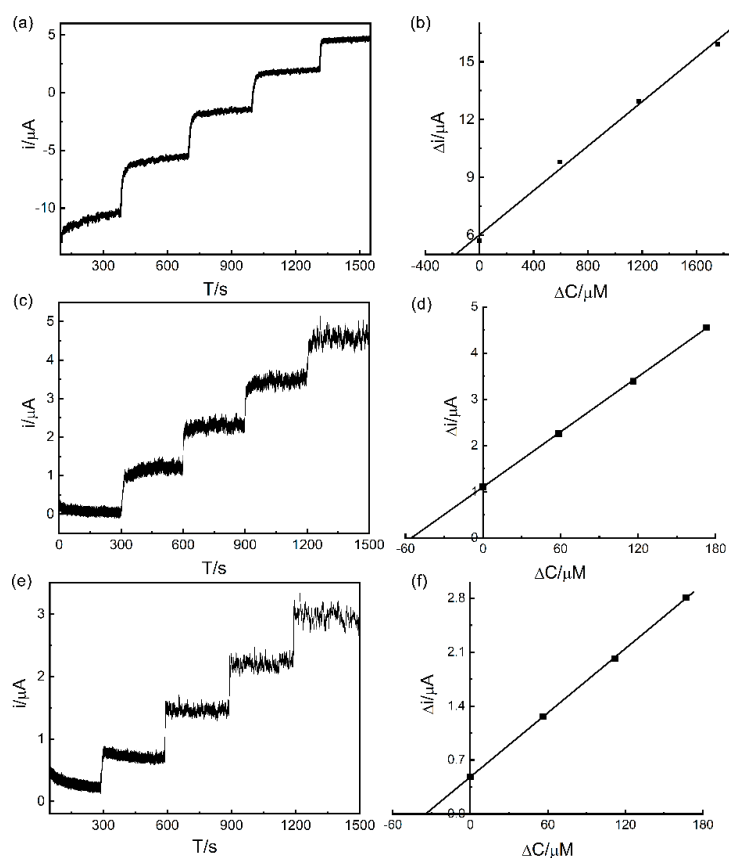


**Figure 16.** (a,c,e) Amperometric response of the sensor under sequential addition of vitamin C tablet, DA injection, and human urine samples, with the AA, DA and UA standard solutions being added three times. (b,d,f) A linear relationship is observed between  $\Delta I$  and  $\Delta C$  for vitamin C tablet, DA injection, and human urine samples on the Pd/MCHS/GCE sensor in PBS solution.

**Table 3.** Results of recoveries of AA and UA in real samples using UV–Vis spectrophotometer.

Samples	Detected		Found		Recovery (%)	
	AA ( $\mu\text{g}$ )	UA ( $\mu\text{M}$ )	AA ( $\mu\text{g}$ )	UA ( $\mu\text{M}$ )	AA	DA
1	10	2.79	$9.81 \pm 0.23$	$2.80 \pm 0.13$	98.10	100.36
2	12	2.99	$12.03 \pm 0.35$	$3.02 \pm 0.18$	100.25	101.00
3	15	3.29	$14.93 \pm 0.44$	$3.35 \pm 0.22$	99.53	101.82
4	20	3.79	$20.03 \pm 0.52$	$3.82 \pm 0.31$	100.15	100.79

### 3. Experimental Section

#### 3.1. Chemicals and Materials

AA, DA, UA, citric acid, calcium nitrate, sucrose, glucose,  $\text{SiO}_2$ ,  $\text{Na}_2\text{PdCl}_4$ , sodium hydroxide (NaOH), resorcol, formaldehyde, and tetraethyl orthosilicate (TEOS) were purchased from Shanghai Macklin Biochemical Co., Ltd. Sodium hydrogen phosphate ( $\text{Na}_2\text{HPO}_4$ ), sodium dihydrogen phosphate ( $\text{NaH}_2\text{PO}_4$ ), phosphoric acid ( $\text{H}_3\text{PO}_4$ ), ammonia ( $\text{NH}_3 \cdot \text{H}_2\text{O}$ ), anhydrous alcohol ( $\text{C}_2\text{H}_6\text{O}$ ), potassium nitrate ( $\text{KNO}_3$ ), and sodium sulfate ( $\text{Na}_2\text{SO}_4$ ) were procured from Tianjin Deen Chemical reagent Co., Ltd., Tianjin, China.  $\text{Al}_2\text{O}_3$  power and all electrodes were purchased from Shanghai Xianren Instrument. All the chemicals and reagents are of analytical grade and used as received without fur-

ther purification. Ultrapure water with a resistivity of 18.2 M $\Omega$  cm was used throughout the experiment.

### 3.2. Synthesis of Pd/MCHS Nanocomposite

Firstly, the Pd/MCHS nanocomposite was synthesized according to our previous report. Briefly, 400 mg SiO<sub>2</sub> was dissolved into a solution of ethanol (70 mL), H<sub>2</sub>O (10 mL), and NH<sub>3</sub>·H<sub>2</sub>O (3 mL) under magnetic stirring for 30 min. Next, Na<sub>2</sub>PdCl<sub>4</sub> (0.265 g) was added in the above solution and stirred for 1 h at 300 rpm. Subsequently, resorcol (0.4 g), formaldehyde (0.56 mL), and tetraethyl orthosilicate (TEOS) (3.46 mL) were added in the solution, and the reaction mixture was continuously stirred for 24 h. After the completion of the reaction, the mixture was consecutively washed with ethanol and ultrapure water to remove the impurities and by-products. Then, the resulting black precipitate was dried overnight at 60 °C under vacuum. The obtained precursor was heated to 800 °C for 2.5 h in an Ar atmosphere at a rate of 2 °C/min. The silica template was removed with NaOH (20%) to obtain the final product, denoted as Pd/MCHS [57].

### 3.3. Characterization and Electrochemical Methods

The morphology of the samples was examined using field emission scanning electron microscopy (FE-SEM; JSM-7610FPlus microscope, JEOL, Tokyo, Japan) and transmission electron microscopy (TEM; Talos F200i microscope, FEI, Hillsboro, OR, USA). The elemental composition and chemical states were investigated through X-ray photoelectron spectroscopy (XPS; Thermo Scientific ESCALAB 250Xi). The crystallographic information was obtained using X-ray diffraction (XRD; Rigaku D/Max-2400). The electrochemical measurements were performed using a CHI 660E electrochemical analyzer with a three-electrode system. A saturated calomel electrode (SCE) and a platinum wire were used as the reference and auxiliary electrodes, respectively, and either GCE or the modified Pd/MCHS/GCE was used as the working electrode. Cyclic voltammetry (CV) and differential pulse voltammetry (DPV) curves were recorded within the potential range of 0.2 to 0.8 V. The electrochemical impedance spectroscopy (EIS) tests were conducted in a 0.1 M KCl solution containing 5 mM Fe(CN)<sub>6</sub><sup>3-/4-</sup> in the frequency range of 0.01–100 Hz. Furthermore, the amperometric response (I-t) curves were generated to assess the anti-interference capability and conduct real sample analysis. These experiments were performed at constant potentials of 0.1 V (AA), 0.42 V (DA), and 0.55 V (UA) under magnetic stirring at 50 rpm/min.

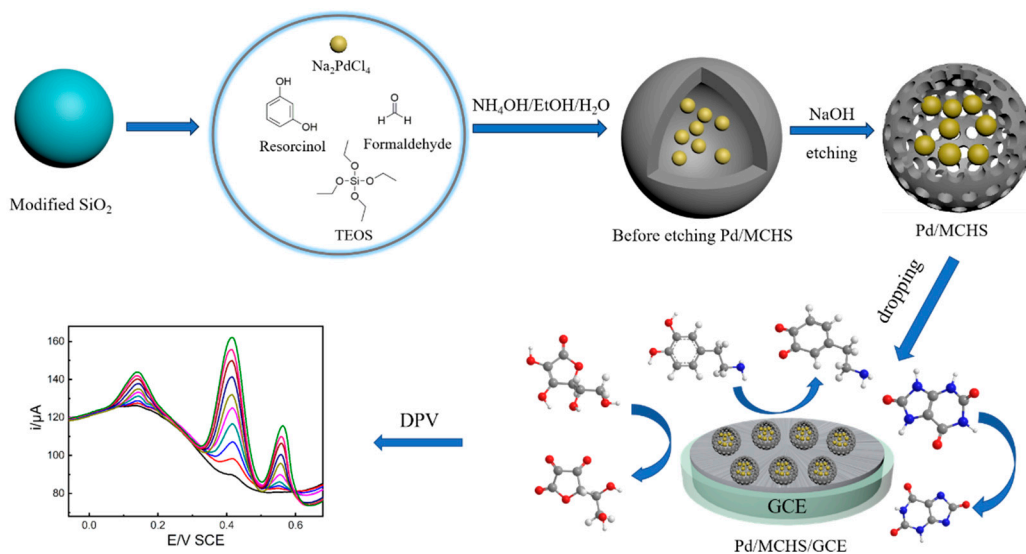
### 3.4. Analysis of Real Samples

Vitamin C tablets and DA injection solution were procured from a local pharmacy, while the UA sample was obtained from a sophomore student at Henan University of Science and Technology. The samples were prepared as follows. Firstly, 0.1 g of the vitamin C tablet was ground and dissolved in 10 mL phosphate-buffered saline (PBS) solution to obtain the actual AA sample. The 20 mg/2 mL DA injection solution and the urine sample were each subjected to a tenfold dilution with 0.1 M PBS (pH = 3.0), without undergoing additional treatment. To obtain the content of AA, DA, and UA in the actual samples, the standard addition method was employed. The recovery percentages were calculated as follows: Recovery (%) = (found/added) × 100%. This approach ensured a rigorous quantitative assessment of the targeted analytes in the real-world samples.

### 3.5. Preparation of Modified Electrode

Firstly, the bare GCE was polished with 1  $\mu$ m and 0.05  $\mu$ m Al<sub>2</sub>O<sub>3</sub> powders, followed by ultrasonic cleaning with 0.5 M H<sub>2</sub>SO<sub>4</sub> and anhydrous ethanol, respectively. Subsequently, 1 mg Pd/MCHS was sonicated in a solution containing 0.5 mL distilled water, 0.5 mL anhydrous ethanol, and 6  $\mu$ L Nafion for 10 min to prepare a homogeneous suspension. Then, the homogeneous suspension (6  $\mu$ L, 1 mg/mL) was dropped on the pretreated GCE and dried using an infrared lamp to prepare the Pd/MCHS/GCE sensor. The preparation

process of the Pd/MCHS/GCE sensor as well as the simultaneous detection of AA, DA, and UA using the fabricated sensor were illustrated in Scheme 1.



**Scheme 1.** Schematic diagram of the preparation of Pd/MCHS/GCE sensor for the detection of AA, DA, and UA.

#### 4. Conclusions

Our study has demonstrated the remarkable properties of the Pd/MCHS/GCE sensor in the molecular recognition of AA, DA and UA, providing a promising avenue for future research. The synergistic combination of MCHS and Pd has contributed to the excellent sensing performance of the electrode sensor and provided a reference approach for the electrochemical detection of small biological molecules. In addition, the non-toxic, profitable and environmentally friendly process further increased the appeal of this new sensing platform. Future studies can focus on the stability and repeatability of these electrochemical sensors over long periods of time and under complex environmental conditions. In addition, we can expand the performance of the Pd/MCHS/GCE sensor in serum and clinical sample applications to provide data references for clinical applications.

**Author Contributions:** W.Z. provided the methodology and modified the manuscript. X.L. (Xijiao Li) wrote the main manuscript text. X.L. (Xiaoxue Liu) and K.S. finished all experiments. H.W. and S.L. prepared materials. J.W. summarized the Characterization section. R.L. and Z.P. prepared all figures and tables. All authors have read and agreed to the published version of the manuscript.

**Funding:** This work was financially supported by the Key Scientific and Technological Project of Henan Province (No. 232102230028), the Key Scientific Research Project of Colleges and Universities of Henan Province (No. 24B150012), and National College Student Innovation and Entrepreneurship Training (No. 202310467017). APC is funded by the Doctoral start-up grant of Henan University of Science and Technology, the funding number is 210010617006.

**Institutional Review Board Statement:** Not applicable.

**Informed Consent Statement:** Informed consent has been obtained from all subjects for this study.

**Data Availability Statement:** Data cannot be shared for ethical/privacy reasons. The data underlying this article cannot be shared publicly due to the privacy of individuals that participated in the study. The data will be shared on reasonable request to the corresponding author. All data generated or analyzed during this study were included in this published article.

**Acknowledgments:** We would like to thank all the reviewers who participated in the reviews.

**Conflicts of Interest:** The authors declare no conflicts of interest.

## References

1. Yang, L.; Wang, A.-J.; Weng, X.; Feng, J.-J. Well-dispersed strawberry-like PtCo nanocrystals/porous N-doped carbon nanospheres for multiplexed assays. *Microchem. J.* **2023**, *187*, 108421. [[CrossRef](#)]
2. Wang, H.; Xie, A.; Li, S.; Wang, J.; Chen, K.; Su, Z.; Song, N.; Luo, S. Three-dimensional g-C<sub>3</sub>N<sub>4</sub>/MWNTs/GO hybrid electrode as electrochemical sensor for simultaneous determination of ascorbic acid, dopamine and uric acid. *Anal. Chim. Acta* **2022**, *1211*, 339907. [[CrossRef](#)] [[PubMed](#)]
3. Wu, P.; Huang, Y.; Zhao, X.; Lin, D.; Xie, L.; Li, Z.; Zhu, Z.; Zhao, H.; Lan, M. MnFe<sub>2</sub>O<sub>4</sub>/MoS<sub>2</sub> nanocomposite as Oxidase-like for electrochemical simultaneous detection of ascorbic acid, dopamine and uric acid. *Microchem. J.* **2022**, *181*, 107780. [[CrossRef](#)]
4. Ma, C.; Xu, P.; Chen, H.; Cui, J.; Guo, M.; Zhao, J. An electrochemical sensor based on reduced graphene oxide/ $\beta$ -cyclodextrin/multiwall carbon nanotubes/polyoxometalate tetracomponent hybrid: Simultaneous determination of ascorbic acid, dopamine and uric acid. *Microchem. J.* **2022**, *180*, 107533. [[CrossRef](#)]
5. Dinesh, B.; Vilian, A.T.E.; Kwak, C.H.; Huh, Y.S.; Saraswathi, R.; Han, Y.-K. The facile and simple synthesis of poly(3,4-ethylenedioxythiophene) anchored reduced graphene oxide nanocomposite for biochemical analysis. *Anal. Chim. Acta* **2019**, *1077*, 150–159. [[CrossRef](#)] [[PubMed](#)]
6. Shen, C.; Chen, Y.; Feng, B.; Chi, H.; Zhang, H. Polypyrrole hollow nanotubes loaded with Au and Fe<sub>3</sub>O<sub>4</sub> nanoparticles for simultaneous determination of ascorbic acid, dopamine, and uric acid. *Chem. Res. Chin. Univ.* **2022**, *38*, 941–948. [[CrossRef](#)]
7. Tchekep, A.G.K.; Suryanarayanan, V.; K Pattanayak, D. Alternative approach for highly sensitive and free-interference electrochemical dopamine sensing. *Carbon* **2023**, *204*, 57–69. [[CrossRef](#)]
8. Thomas, J.; Anitha, P.K.; Thomas, T.; Thomas, N. BaZrO<sub>3</sub> based non enzymatic single component single step ceramic electrochemical sensor for the picomolar detection of dopamine. *Ceram. Int.* **2022**, *48*, 7168–7182. [[CrossRef](#)]
9. Chakkarapani, L.D.; Arumugam, S.; Brandl, M. Layer-by-layer sensor architecture of polymers and nanoparticles for electrochemical detection of uric acid in human urine samples. *Mater. Today Chem.* **2021**, *22*, 100561. [[CrossRef](#)]
10. Sha, R.; Vishnu, N.; Badhulika, S. MoS<sub>2</sub> based ultra-low-cost, flexible, non-enzymatic and non-invasive electrochemical sensor for highly selective detection of Uric acid in human urine samples. *Sens. Actuators B Chem.* **2019**, *279*, 53–60. [[CrossRef](#)]
11. Wu, S.; Wang, H.; Zhao, B.; Cao, T.; Ma, J.; Liu, L.; Tong, Z. Construction of cationic polyfluorinated azobenzene/reduced graphene oxide for simultaneous determination of dopamine, uric acid and ascorbic acid. *Talanta* **2022**, *237*, 122986. [[CrossRef](#)] [[PubMed](#)]
12. Zhang, H.; Liu, S. Electrochemical sensors based on nitrogen-doped reduced graphene oxide for the simultaneous detection of ascorbic acid, dopamine and uric acid. *J. Alloys Compd.* **2020**, *842*, 155873. [[CrossRef](#)]
13. Zhu, Q.; Bao, J.; Huo, D.; Yang, M.; Hou, C.; Guo, J.; Chen, M.; Fa, H.; Luo, X.; Ma, Y. 3D Graphene hydrogel-gold nanoparticles nanocomposite modified glassy carbon electrode for the simultaneous determination of ascorbic acid, dopamine and uric acid. *Sens. Actuators B Chem.* **2017**, *238*, 1316–1323. [[CrossRef](#)]
14. Kunpatee, K.; Traipop, S.; Chailapakul, O.; Chuanwatanakul, S. Simultaneous determination of ascorbic acid, dopamine, and uric acid using graphene quantum dots/ionic liquid modified screen-printed carbon electrode. *Sens. Actuators B Chem.* **2020**, *314*, 128059. [[CrossRef](#)]
15. Jothi, L.; Neogi, S.; Jaganathan, S.K.; Nageswaran, G. Simultaneous determination of ascorbic acid, dopamine and uric acid by a novel electrochemical sensor based on N<sub>2</sub>/Ar RF plasma assisted graphene nanosheets/graphene nanoribbons. *Biosens. Bioelectron.* **2018**, *105*, 236–242. [[CrossRef](#)] [[PubMed](#)]
16. Peng, Y.; Shao, F.; Guo, K.; Zhuo, H.; Wang, Y.; Xie, X.; Tao, Y. SiQDs/Cu- $\beta$ -CD nanoclusters: A fluorescence probe for the mutual non-interference detection of uric acid and l-cysteine under alkaline conditions. *Inorg. Chem. Commun.* **2022**, *143*, 109765. [[CrossRef](#)]
17. Liu, X.; Yu, W.; Mu, X.; Zhang, W.; Wang, X.; Gu, Q. A fluorescence probe based on carbon dots for determination of dopamine utilizing its self-polymerization. *Spectrochim. Acta Part A Mol. Biomol. Spectrosc.* **2023**, *287*, 122112. [[CrossRef](#)]
18. Chen, X.; Chen, J.; Wang, F.; Xiang, X.; Luo, M.; Ji, X.; He, Z. Determination of glucose and uric acid with bienzyme colorimetry on microfluidic paper-based analysis devices. *Biosens. Bioelectron.* **2012**, *35*, 363–368. [[CrossRef](#)] [[PubMed](#)]
19. Porto, I.S.A.; Santos Neto, J.H.; dos Santos, L.O.; Gomes, A.A.; Ferreira, S.L.C. Determination of ascorbic acid in natural fruit juices using digital image colorimetry. *Microchem. J.* **2019**, *149*, 104031. [[CrossRef](#)]
20. Wang, X.; Li, L.; Li, Z.; Wang, J.; Fu, H.; Chen, Z. Determination of ascorbic acid in individual liver cancer cells by capillary electrophoresis with a platinum nanoparticles modified electrode. *J. Electroanal. Chem.* **2014**, *712*, 139–145. [[CrossRef](#)]
21. Costa, B.M.C.; Prado, A.A.; Oliveira, T.C.; Bressan, L.P.; Munoz, R.A.A.; Batista, A.D.; da Silva, J.A.F.; Richter, E.M. Fast methods for simultaneous determination of arginine, ascorbic acid and aspartic acid by capillary electrophoresis. *Talanta* **2019**, *204*, 353–358. [[CrossRef](#)] [[PubMed](#)]
22. Kand'ár, R.; Drábková, P.; Hampl, R. The determination of ascorbic acid and uric acid in human seminal plasma using an HPLC with UV detection. *J. Chromatogr. B* **2011**, *879*, 2834–2839. [[CrossRef](#)] [[PubMed](#)]
23. Sun, C.-L.; Lai, S.-Y.; Tsai, K.-J.; Wang, J.; Zhou, J.; Chen, H.-Y. Application of nanoporous core-shell structured multi-walled carbon nanotube-graphene oxide nanoribbons in electrochemical biosensors. *Microchem. J.* **2022**, *179*, 107586. [[CrossRef](#)]
24. Wang, Y.; Zhao, P.; Gao, B.; Yuan, M.; Yu, J.; Wang, Z.; Chen, X. Self-reduction of bimetallic nanoparticles on flexible MXene-graphene electrodes for simultaneous detection of ascorbic acid, dopamine, and uric acid. *Microchem. J.* **2023**, *185*, 108177. [[CrossRef](#)]

25. Mahanthappa, M.; Duraisamy, V.; Arumugam, P.; Senthil Kumar, S.M. Simultaneous determination of ascorbic acid, dopamine, uric acid, and acetaminophen on N, P-doped hollow mesoporous carbon nanospheres. *ACS Appl. Nano Mater.* **2022**, *5*, 18417–18426. [[CrossRef](#)]
26. Tang, T.; Zhou, M.; Lv, J.; Cheng, H.; Wang, H.; Qin, D.; Hu, G.; Liu, X. Sensitive and selective electrochemical determination of uric acid in urine based on ultrasmall iron oxide nanoparticles decorated urchin-like nitrogen-doped carbon. *Colloids Surf. B Biointerfaces* **2022**, *216*, 112538. [[CrossRef](#)] [[PubMed](#)]
27. Feng, J.; Li, Q.; Cai, J.; Yang, T.; Chen, J.; Hou, X. Electrochemical detection mechanism of dopamine and uric acid on titanium nitride-reduced graphene oxide composite with and without ascorbic acid. *Sens. Actuators B Chem.* **2019**, *298*, 126872. [[CrossRef](#)]
28. Lin, K.-C.; Tsai, T.-H.; Chen, S.-M. Performing enzyme-free H<sub>2</sub>O<sub>2</sub> biosensor and simultaneous determination for AA, DA, and UA by MWCNT–PEDOT film. *Biosens. Bioelectron.* **2010**, *26*, 608–614. [[CrossRef](#)]
29. Yang, G.; Kuwahara, Y.; Mori, K.; Louis, C.; Yamashita, H. Pd–Cu alloy nanoparticles confined within mesoporous hollow carbon spheres for the hydrogenation of CO<sub>2</sub> to formate. *J. Phys. Chem. C* **2021**, *125*, 3961–3971. [[CrossRef](#)]
30. Zheng, Y.; Chen, S.; Zhang, K.A.I.; Guan, J.; Yu, X.; Peng, W.; Song, H.; Zhu, J.; Xu, J.; Fan, X.; et al. Template-free construction of hollow mesoporous carbon spheres from a covalent triazine framework for enhanced oxygen electroreduction. *J. Colloid Interface Sci.* **2022**, *608*, 3168–3177. [[CrossRef](#)]
31. Song, D.; An, S.; Lu, B.; Guo, Y.; Leng, J. Arylsulfonic acid functionalized hollow mesoporous carbon spheres for efficient conversion of levulinic acid or furfuryl alcohol to ethyl levulinate. *Appl. Catal. B Environ.* **2015**, *179*, 445–457. [[CrossRef](#)]
32. Zhang, L.; Yu, X.; Lv, L.; Zhu, P.; Zhou, F.; Li, G.; Sun, R.; Wong, C. Ultrathin manganese dioxide nanosheets grown on mesoporous carbon hollow spheres for high performance asymmetrical supercapacitors. *ACS Appl. Energy Mater.* **2018**, *1*, 5402–5409. [[CrossRef](#)]
33. Lin, Y.-S.; Lin, K.-S.; Mdllovu, N.V.; Kung, P.-Y.; Jeng, U.S. Thermal-/pH-triggered hollow mesoporous carbon nanocarrier for NIR-responsive drug release. *Biomater. Adv.* **2023**, *151*, 213477. [[CrossRef](#)] [[PubMed](#)]
34. Wang, B.; Xia, Y.; Bai, J.; Yuan, G.; Ma, H. Facile synthesis of MoS<sub>2</sub> confined in yolk-shell hollow mesoporous carbon spheres with enhanced polysulfide binding for high-rate Li-S batteries. *J. Alloys Compd.* **2024**, *970*, 172617. [[CrossRef](#)]
35. Liu, P.; Liu, W.; Huang, Y.; Li, P.; Yan, J.; Liu, K. Mesoporous hollow carbon spheres boosted, integrated high performance aqueous Zn-Ion energy storage. *Energy Storage Mater.* **2020**, *25*, 858–865. [[CrossRef](#)]
36. Wang, Z.; Zhao, H.; Chen, K.; Li, H.; Lan, M. Sandwich-type electrochemical aptasensor based on hollow mesoporous carbon spheres loaded with porous dendritic Pd@Pt nanoparticles as signal amplifier for ultrasensitive detection of cardiac troponin I. *Anal. Chim. Acta* **2021**, *1188*, 339202. [[CrossRef](#)] [[PubMed](#)]
37. Baca, M.; Cendrowski, K.; Banach, P.; Michalkiewicz, B.; Mijowska, E.; Kalenczuk, R.J.; Zielinska, B. Effect of Pd loading on hydrogen storage properties of disordered mesoporous hollow carbon spheres. *Int. J. Hydrogen Energy* **2017**, *42*, 30461–30469. [[CrossRef](#)]
38. Ahn, S.; Park, K.; Lee, K.R.; Haider, A.; Nguyen, C.V.; Jin, H.; Yoo, S.J.; Yoon, S.; Jung, K.-D. Atomically dispersed Ru(III) on N-doped mesoporous carbon hollow spheres as catalysts for CO<sub>2</sub> hydrogenation to formate. *Chem. Eng. J.* **2022**, *442*, 136185. [[CrossRef](#)]
39. Gai, H.-Y.; Wang, X.-K.; Huang, M.-H. Catalytic Activity Analysis of uniform palladium nanoparticles anchored on nitrogen-doped mesoporous carbon spheres for oxygen reduction reaction. *Chin. J. Anal. Chem.* **2021**, *49*, e21096–e21103. [[CrossRef](#)]
40. Yang, C.; Li, K.; Wang, J.; Zhou, S. Selective hydrogenation of phenol to cyclohexanone over Pd nanoparticles encaged hollow mesoporous silica catalytic nanoreactors. *Appl. Catal. A Gen.* **2021**, *610*, 117961. [[CrossRef](#)]
41. Dong, L.; Li, Y.; Li, J.; Guan, Y.; Chen, X.; Zhang, D.; Wang, Z. Mesoporous carbon hollow spheres encapsulated phase change material for efficient emulsification of high-viscosity oil. *J. Hazard. Mater.* **2023**, *451*, 131112. [[CrossRef](#)]
42. Sun, S.; Zhang, Y.; Li, H. N-doped hollow carbon nanospheres anchored Pd NPs for mild selective hydrodeoxygenation of bio-models. *Fuel* **2023**, *352*, 128929. [[CrossRef](#)]
43. Zhu, Y.; Wang, F.; Fan, M.; Zhu, Q.; Dong, Z. Ultrafine Pd nanoparticles immobilized on N-doped hollow carbon nanospheres with superior catalytic performance for the selective oxidation of 5-hydroxymethylfurfural and hydrogenation of nitroarenes. *J. Colloid Interface Sci.* **2019**, *553*, 588–597. [[CrossRef](#)]
44. Song, Z.-Y.; Ma, Y.; Ye, J.-S. Electrochemical sensors for simultaneous determination of small biomolecules by 3D layered hollow honeycomb-like Ni-NiO@CPVP modified glassy carbon electrode. *Chin. J. Anal. Chem.* **2020**, *48*, e20047–e20055. [[CrossRef](#)]
45. Wang, Y.; Dai, Q.; Yang, L.; Liu, Y.; Yu, C.; Yao, C.; Xu, X. One-pot and surfactant-free synthesis of N-doped mesoporous carbon spheres for the sensitive and selective screening of small biomolecules. *J. Electroanal. Chem.* **2020**, *873*, 114462. [[CrossRef](#)]
46. Ognjanovic, M.; Stankovi, D.M.; Jovic, M.; Krsti, M.; Lesch, A.; Girault, H.H.; Antic, B.V. Inkjet-printed carbon nanotube electrodes modified with dimercaptosuccinic acid-capped Fe<sub>3</sub>O<sub>4</sub> nanoparticles on reduced graphene oxide nanosheets for single-drop determination of trifluoperazine. *Appl. Nano Mater.* **2020**, *3*, 4654–4662. [[CrossRef](#)]
47. Petković, B.B.; Ognjanović, M.; Krstić, M.; Stanković, V.; Babincev, L.; Pergal, M.; Stanković, D.M. Boron-doped diamond electrode as efficient sensing platform for simultaneous quantification of mefenamic acid and indomethacin. *Diam. Relat. Mater.* **2020**, *105*, 107785. [[CrossRef](#)]
48. Martínez-Hincapié, R.; Wegner, J.; Anwar, M.U.; Raza-Khan, A.; Franzka, S.; Kleszczynski, S.; Čolić, V. The determination of the electrochemically active surface area and its effects on the electrocatalytic properties of structured nickel electrodes produced by additive manufacturing. *Electrochim. Acta* **2024**, *476*, 143663. [[CrossRef](#)]

49. Zhang, L.; Zhang, J. 3D hierarchical bayberry-like Ni@carbon hollow nanosphere/rGO hybrid as a new interesting electrode material for simultaneous detection of small biomolecules. *Talanta* **2018**, *178*, 608–615. [[CrossRef](#)]
50. Li, Q.; Huo, C.; Yi, K.; Zhou, L.; Su, L.; Hou, X. Preparation of flake hexagonal BN and its application in electrochemical detection of ascorbic acid, dopamine and uric acid. *Sens. Actuators B Chem.* **2018**, *260*, 346–356. [[CrossRef](#)]
51. Ding, S.; Dai, M.; Su, X.; Guo, D.; Bian, L.; Liu, X. Electrochemically functionalized carbon cloth for simultaneous determination of ascorbic acid, dopamine, and uric acid. *J. Electroanal. Chem.* **2022**, *915*, 116349. [[CrossRef](#)]
52. Yang, L.; Liu, D.; Huang, J.; You, T. Simultaneous determination of dopamine, ascorbic acid and uric acid at electrochemically reduced graphene oxide modified electrode. *Sens. Actuators B Chem.* **2014**, *193*, 166–172. [[CrossRef](#)]
53. Colín-Orozco, E.; Corona-Avendaño, S.; Ramírez-Silva, M.T.; Romero-Romo, M.; Palomar-Pardavé, M. On the electrochemical oxidation of dopamine, ascorbic acid and uric acid onto a bare carbon paste electrode from a 0.1 M NaCl aqueous solution at pH 7. *Int. J. Electrochem. Sci.* **2012**, *7*, 6097–6105. [[CrossRef](#)]
54. Colín-Orozco, E.; Ramírez-Silva, M.T.; Corona-Avendaño, S.; Romero-Romo, M.; Palomar-Pardavé, M. Electrochemical quantification of dopamine in the presence of ascorbic acid and uric acid using a simple carbon paste electrode modified with SDS micelles at pH 7. *Electrochim. Acta* **2012**, *85*, 307–313. [[CrossRef](#)]
55. Du, J.; Yue, R.; Ren, F.; Yao, Z.; Jiang, F.; Yang, P.; Du, Y. Novel graphene flowers modified carbon fibers for simultaneous determination of ascorbic acid, dopamine and uric acid. *Biosens. Bioelectron.* **2014**, *53*, 220–224. [[CrossRef](#)]
56. Wang, C.; Du, J.; Wang, H.; Zou, C.E.; Jiang, F.; Yang, P.; Du, Y. A facile electrochemical sensor based on reduced graphene oxide and Au nanoplates modified glassy carbon electrode for simultaneous detection of ascorbic acid, dopamine and uric acid. *Sens. Actuators B Chem.* **2014**, *204*, 302–309. [[CrossRef](#)]
57. Peng, Z.; Wang, H.; Zhou, L.; Wang, Y.; Gao, J.; Liu, G.; Redfern, S.A.T.; Feng, X.; Lu, S.; Li, B.; et al. Hollow carbon shells enhanced by confined ruthenium as cost-efficient and superior catalysts for the alkaline hydrogen evolution reaction. *J. Mater. Chem. A* **2019**, *7*, 6676–6685. [[CrossRef](#)]

**Disclaimer/Publisher’s Note:** The statements, opinions and data contained in all publications are solely those of the individual author(s) and contributor(s) and not of MDPI and/or the editor(s). MDPI and/or the editor(s) disclaim responsibility for any injury to people or property resulting from any ideas, methods, instructions or products referred to in the content.